Generalized Spatio-Temporal Model of Backsheet Degradation From Field Surveys of Photovoltaic Modules

Yu Wang, Wei-Heng Huang, Andrew Fairbrother, Lucas S. Fridman, Alan J. Curran, Nicholas R. Wheeler, Sophie Napoli, Adam W. Hauser, Scott Julien, Xiaohong Gu, Gregory S. O'Brien, Kai-Tak Wan, Liang Ji, Michael D. Kempe, Kenneth P. Boyce, Roger H. French, and Laura S. Bruckman

***Abstract*—Photovoltaic (PV) module backsheets degrade at different rates because of the specific polymeric materials and the local exposure environments of the installations. Studies of real-world backsheet degradation provide valuable information to understand backsheet degradation and failure. Field surveys of PV module backsheets were conducted on 1310 modules in four commercial PV power plant sites with different exposure times. The backsheet's local exposure environment is determined by its location along the rack length and depth, the modules' elevation above the ground, and the ground cover albedo. Backsheets that are installed at the ends of the module rack length exhibit larger degradation rates (with yellowness index difference of 1.14 $\pm$ 0.45 and 7.80 $\pm$ 1.3 for backsheets of poly (ethylene terephthalate) and poly (ethylene naphthalate) as the air-side layer, respectively) than backsheets in the center section of the rack. A generalized spatio-temporal model was developed to predict the large-scale backsheet degradation of different backsheet polymers across time/age and location in the PV power plant rack. The model utilizes a cubic-spline relationship between backsheet degradation and rack length, and a quadratic relationship between backsheet discoloration and rack depth. This generalized spatio-temporal model predicts the outdoor backsheet degradation with an adjusted-R^2 range between 0.31 to 0.89. The similarity between this model and the spatial variation of the rear-side irradiance, indicates that the irradiance plays a significant role in outdoor backsheet degradation. The generalized spatio-temporal model can be used to evaluate large scale PV backsheet performance, as well as a guidance for PV site designers and operations and maintenance crews.**

***Index Terms*—Backsheet degradation, field survey, photovoltaic (PV) module, spatio-temporal model.**

I. Introduction

PREDICTION of photovoltaic (PV) modules degradation under real-world exposure conditions and environments is needed to support the continued growth of PV power plant installations. Backsheets play a significant role in maintaining the high performance of PV modules and providing necessary safety guarantees [1]. Degradation and failure of backsheets compromise the lifetime of PV modules. Understanding real-world degradation of PV module backsheets is essential to enable informed future material choices for reliable and durable backsheets.

Backsheet polymers degrade because of a variety of stressors including ultraviolet (UV) light, temperature, and humidity. Commonly observed backsheet degradation includes discoloration, burn spots, blistering, cracking, and delamination [2]–[4]. In the 2017 IEA-PVPS report of field surveys of 1211 modules from seven countries and three Köppen–Geiger climatic zones [5], 9% of studied c-Si modules showed backsheet degradation [6]. A series of field studies of approximately 1.5 million PV module backsheets exposed to different climates showed 9% of backsheets with visable degradation of the air-side of various materials including poly(vinylidene fluoride) (PVDF), poly(ethylene-terephthalate) (PET), and fluoroethylene vinyl ether [7]. Power loss, water ingress, and current leakage were also observed on some PV modules with defective or degraded backsheets [8]. Polyamide (PA) backsheets (PA/PA/PA), which passed standard qualification testing, showed severe cracking after five years of exposure in Italy [9]. Delamination was also observed on a polyvinyl fluoride (PVF)/PET/PVF backsheets at the interface between the

Manuscript received April 11, 2019; revised June 23, 2019; accepted July 3, 2019. Date of publication August 2, 2019; date of current version August 22, 2019. This work was supported by the Department of Energy's Office of Energy Efficiency and Renewable Energy (EERE), Solar Energy Technologies Office PREDICTS2 program (DE-EE0007143). *(Corresponding author: Laura S. Bruckman.)*

Y. Wang, L. S. Fridman, A. J. Curran, N. R. Wheeler, R. H. French, and L. S. Bruckman are with the SDLE Research Center, Materials Science Engineering, Case Western Reserve University, Cleveland, OH 44106 USA (e-mail: yxw880@case.edu; lsf21@case.edu; ajc269@case.edu; nrw16@case.edu; rxf131@case.edu; lsh41@case.edu).

W. H. Huang is with the SDLE Research Center, Department of Materials Science and Engineering, Case Western Reserve University, Cleveland, OH 44106 USA, and also with the Department of Statistics, Feng Chia University, Taichung 40724, Taiwan, R.O.C. (e-mail: wxh272@case.edu).

A. Fairbrother and X. Gu are with the Engineering Laboratory, National Institute of Standards and Technology, Gaithersburg, MD 20899 USA (e-mail: andrew.fairbrother@nist.gov; xiaohong.gu@nist.gov).

S. Napoli, A. W. Hauser, and G. S. O. Brien are with the Fluoropolymers R&D, Arkema, Inc., King of Prussia, PA 19406 USA (e-mail: sophie.napoli@arkema.com; adam.hauser@arkema.com; greg.obrien@arkema.com).

S. Julien and K. T. Wan are with the Department of Mechanical and Industrial Engineering, Northeastern University, Boston, MA 02115 USA (e-mail: julien.s@husky.neu.edu; ktwan@coe.neu.edu).

L. Ji and K. P. Boyce are with the Renewable Energy, Underwriters Laboratories Inc., Northbrook, IL 60062 USA (e-mail: liang.ji@ul.com; kenneth.p.boyce@ul.com).

M. D. Kempe is with the Photovoltaics Research, National Renewable Energy Laboratory, Golden, CO 80401 USA (e-mail: michael.kempe@nrel.gov).

Color versions of one or more of the figures in this paper are available online at http://ieeexplore.ieee.org.

Digital Object Identifier 10.1109/JPHOTOV.2019.2928700

air-side PVF layer and core PET layers after 12 years exposure in Spain [10]. Although the occurrence of backsheet degradation is lower than other reported types of PV degradation, degraded backsheets induce severe safety issues and can accelerate the degradation of other PV module components [11], [12]. For instance, cracked backsheets provide pathways for UV exposure, oxygen permeation, and water ingress, which may induce encapsulant degradation, corrosion of metallization, and sharply decrease the insulation resistance or protection [13]. Surveying real-world degradation in fielded modules is pivotal to enable our understanding of backsheet degradation under real-world exposure conditions and for accurate lifetime prediction [2].

Comprehensive field evaluations of backsheet degradation lack in comparison with the large number of field studies of front-side PV module degradation modes, such as soiling, cell cracking, snail trails, and encapsulant yellowing [14]–[17]. Polymeric backsheets yellow, or change color, associated with degradation because of various environmental factors, such as UV irradiance. The yellowness index (YI) is a sensitive indicator of degradation. In some cases, discoloration of PV backsheets may be related to decrease of mechanical properties and module power output [18]. Gambogi *et al*. showed that the PET-based backsheets on a roof in Japan had a higher degree of discoloration at the lateral *rack ends* of the PV array relative to the center of the array [19], that demonstrates the occurrence of spatially nonuniform backsheet degradation. In recent work, a similar finding was observed in poly(ethylene naphthalate) (PEN) after four years of exposure in Maryland, USA [20]. The greater backsheet yellowing at the ends of a rack compared with the center of the rack shows that the edges of a PV power plant installation are potential failure areas for PV power plants.

The nonuniform backsheet degradation is assumed to depend on the rear-side irradiance distribution [20]. In bifacial module research, the energy gained from back-side illumination was calculated with physical models of rear-side irradiance [21], [22]. The rear-side irradiance distribution is affected by PV power plant site design parameters, such as rack clearance (elevation from ground to lowest part of array), module orientation, rack tilt angle and height, and rack-to-rack spacing in the array [22]. However, it is the UV component of the incident irradiance, rather than the full spectrum light, that is the main driver of backsheet degradation [20]. The UV component of the irradiance changes dramatically based on the ground cover [20], [23]. In addition, PV backsheet degradation is a complex combination of polymeric material interactions combined with the synergistic effects of temperature, humidity, light, and other external stressors [11].

Data-driven statistical models are useful to find the quantitative relationship between a response and predictors [24]. Predictive models have been used to characterize the effect of stressors (predictors, e.g., spatial location and exposure time) on material properties (response, e.g., YI) as in a backsheet field survey study. The combination of predictive models and material science allows the understanding of material scientists to predict the performance of backsheet degradation [25]–[29]. Therefore, a predictive model based on real-world backsheet degradation data from field surveys is necessary to realistically predict their lifetime performance and degradation and failure modes; especially the variations in backsheet performance with location in the PV power plant's array, such as rack end versus the center of a PV module rack.

TABLE I
FIELD SURVEY SITE INFORMATION

Site	I	II	III	IV
Climatic Zone	Dfb: Humid continental		Cfa: Humid subtropical	
Brand	K	L	M, N	O
Air-side Material	PVDF	PA	PET, PET	PEN
Module Dimension (m)	1.96×0.992	1.65×0.992	1.67×0.994, 1.66×0.990	1.64×0.993
Ground Cover	Grass	Grass	Grass	Gray rock
Mount Configuration	Landscape	Landscape	Portrait	Landscape
Installation Year	Nov, 2013	Feb, 2012	Sep, 2014	Aug, 2012
Field Survey Year	2017	2017	2016-2018, 2017-2018	2016
Rack Column Number	82	80	26	48
Rack Row Number	4	5	2	5
Clearance (m)	1.035	0.6	0.6	0.6
Tilt Angle (°)	28	20	20	20

Note: Cfa: $-3 \leq T_{\min} \leq 18\,^{\circ}\mathrm{C}$, $T_{\max} \geq 22\,^{\circ}\mathrm{C}$; Dfb: $T_{\min} \geq -38^{\circ}\mathrm{C}$, $T_{\max} \leq 22\,^{\circ}\mathrm{C}$, precipitation more evenly distributed throughout year.

In this study, the degradation of five types of backsheets, exposed in four real-world PV power plants, located in two climatic zones were evaluated with nondestructive optical and spectroscopic measurements. YI is used as a sensitive response to monitor for changes in backsheet properties over the space of a field [30]. Here, we develop a generalized spatio-temporal model to predict the YI of the backsheets of polymeric materials that differ in different climatic zones, by fitting the model to data collected from various field surveys.

II. EXPERIMENT AND METHOD

A. PV Field Survey

1) PV Field Description: A total of 1310 modules of five brands from four commercial PV sites located in two different Köppen–Geiger [5] climatic zones were evaluated by field survey (Table I). The initial field survey on PV modules with an air-side backsheet polymer of PEN in Maryland (site IV) [20] is also included.

PV power plant sites are described spatially as a series of racks. These racks are each characterized by the parameters as follows: A horizontal row of modules in the rack (PV modules with the same height in one rack), a vertical column of modules in the rack (PV modules located in the row which are at the same vertical position), the tilt angle of the rack (the angle of

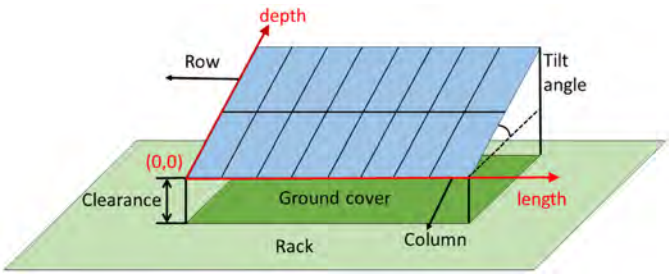

Fig. 1. Schematic diagram of a PV module rack in a PV power plant site that shows the module rows and columns along the rack length and rack depth, and the clearance and tilt angle of the modules. The "(0,0)" represents the origin of the reference coordinate system of the rack while looking from the backsheet side of the rack.

the rack to the horizontal ground) and the ground cover type (Fig. 1). The PV module columns in a rack signify the number of modules installed from left to right, as viewed from the back side of the rack (i.e., the air-side backsheet of the PV module).

2) Backsheet Characterization: The air-side material of backsheets in site I to III was identified by the use of an Agilent 4300 Handheld Portable attenuated total reflection Fourier-transform infrared spectroscopy (ATR-FTIR) spectrometer with a diamond crystal. Backsheets were further characterized by the use of nondestructive spectroscopic evaluation of the YI according to ASTM E313 [30] (HunterLab MiniScan colorimeter) with D65/10 illuminant and observer. The study protocol for the backsheet field survey called for backsheets at module column of the 1st, 15th, 30th, 45th, 60th, and 82nd for site I, or 80th for site II in all rows were evaluated (again counted from left to right, viewing the modules from the back side). For both sites I and II, three measurements were taken on each backsheet at the corner, center, and near the junction box. For site III, there are two PV module brands (M and N), each in different racks in this PV power plant site, and measurements were conducted on every backsheet in one rack for each PV module brand, with a total of 18 measurements taken at the top, center, and bottom for each backsheet of each brand. At site III, recurring field surveys were conducted, once each year for a period of three and two years respectively on module brands M and N. The measurement locations were converted to the length and depth, which indicated the distance (m) from the original point "(0,0)" in the rack (Fig. 1) to the measurement point. The backsheet material identification and characterization for site IV was done in a similar manner and is summarized in [20]. For site IV, every other module was measured from one of the rack, which means that the end module at the other end was not measured. Therefore, the data from the first column module was duplicated for the 48th column.

B. Spatio-Temporal Model Development

A generalized additive model (GAM) is a type of generalized linear additive model that enables to fit a nonlinear function for each predictor that retain the desirable properties of additive models [31]. This approach uses a linear combination of spline bases to estimate the relationship between responses and predictors. A GAM can be described as follows:

$$Y = f_1(X_1) + f_2(X_2) + \cdots + f_m(X_m) + \epsilon \tag{1}$$

where Y is a response (i.e., YI), $X_1, X_2, \ldots, X_m$ are predictors (i.e. length, depth, and time) and $f_i(X_i)$, $i = 1, 2, \ldots, m$ are corresponding nonlinear functions, commonly splines, for each predictor, and ϵ is the error term. A general basis function can be represented as follows:

$$\begin{aligned} f(X) &= \beta_0 + \beta_1 b_1(X) + \beta_2 b_2(X) + \cdots + \beta_q b_q(X) \\ &= \sum_{i=0}^{q} \beta_i b_i(X) \end{aligned} \tag{2}$$

where $b_0(X) = 1, b_1(X), \ldots, b_q(X)$ are the basis functions, q is the number of basis functions, and β_q's are coefficients. Therefore, a cubic spline with K knots can be written in the basis function as follows:

$$\begin{aligned} f(X) = \beta_0 + \beta_1 X + \beta_2 X^2 + \beta_3 X^3 + \beta_4 (X - a_1)_+^3 \\ + \beta_5 (X - a_2)_+^3 \cdots + \beta_{K+3} (X - a_K)_+^3 \end{aligned} \tag{3}$$

where $(X - a)_+^3 = (X - a)^3$ if $X > a$, or 0 otherwise, and $a_1, \ldots, a_k$ are knots. The knots of the spline define the points at which the data is partitioned into distinct regions, and a cubic polynomial function is built in each region between the knots. Constraints are enforced on the splines where they meet at a knot. Here the splines are constrained to remain continuous, with continuous first and second derivatives, at each of the knots.

A generalized spatio-temporal model was developed, using a GAM, with YI as the response, and time, backsheet spatial location, air-side material, and ground cover as predictors, to predict the aging performance of backsheets. A cubic spline and a quadratic function were used for the length predictor and the depth predictor, respectively, to capture the nonlinear relationships between the YI and the spatial predictors. The air-side material and ground cover are treated as indicator variables. The field survey dataset was split into a training set and a testing set. The generalized spatio-temporal model was fit on the training set which encompasses 80% of the dataset and tested on the 20% of the data that remains.

The generalized spatio-temporal model was validated with a tenfold cross-validation method. The k-fold cross validation method, for $k = 10$, involves random partition of the data into ten groups of approximately equal size and using the first group as the validation set and the remaining nine groups as the training set, and performing this process ten times. This process results in ten estimates of test error, $\text{MSE}_1, \ldots, \text{MSE}_{10}$. The root average of these ten test errors is computed by, $\text{RMSE} = \sqrt{\sum_{i=1}^{10} \text{MSE}_i / 10}$. If the value of test RMSE is relatively small compared with range of raw data, then the model is not over-fitting. In this study, the performance of the generalized spatio-temporal model was assessed through calculation of the RMSE and adjusted R^2.

III. Results

A. Backsheet Identification and Characterization

The air-side materials of the five studied backsheets in sites I–IV were identified by their ATR-FTIR spectra and the results shown in Table I. Both uniform and nonuniform backsheet degradation were observed across the different PV sites surveyed and across the different backsheet air-side polymer materials, exposure times, and site designs. Fig. 2 shows YI values of backsheets with different spatial locations in sites I–IV. The backsheets in sites I, II, and III with PV module brand M showed similar YI values and uniform degradation across the whole racks surveyed. However, higher YI of brand N PV module backsheets at the two ends of the rack were observed during the two field survey of site III in June 2017 and July 2018 [the second survey result was shown in Fig. 2(d)]. Moreover, backsheets in the PV power plant site IV also exhibited spatially nonuniform degradation based on their location within the rack. The differences of YI for the backsheets at the center of the PV rack compared with the YI at the rack ends we refer to as the rack length "end effect".

B. Generalized Spatio-Temporal Model

In the generalized spatio-temporal model, if the rack "end effect" is observed, then the locations of knots along the rack length direction are set at the positions where the "end effect" occurs and the positions are determined by the use of the "segmented" R package [32]. For the sites where no "end effect" can be detected, the locations of knots are set at 20% and 80% of the total length of the row. The generalized spatio-temporal model can be represented as follows:

$$Y = M_i \times G_i \times (\beta_0 + \beta_1 L + \beta_2 L^2 + \beta_3 L^3 + \beta_4 (L - a_1)_+^3 + \beta_5 (L - a_2)_+^3 + \beta_6 D + \beta_7 D^2 + \beta_8 t) + \epsilon \quad (4)$$

where Y represents YI, M_i is the backsheet air-side material

$$M_1 = \begin{cases} 1 & \text{if air-side material is PVDF} \\ 0 & \text{otherwise} \end{cases}$$

$$M_2 = \begin{cases} 1 & \text{if air-side material is PA} \\ 0 & \text{otherwise} \end{cases}$$

$$M_3 = \begin{cases} 1 & \text{if air-side material is PET (brand M)} \\ 0 & \text{otherwise} \end{cases}$$

$$M_4 = \begin{cases} 1 & \text{if air-side material is PET (brand N)} \\ 0 & \text{otherwise} \end{cases}$$

$$M_5 = \begin{cases} 1 & \text{if air-side material is PEN} \\ 0 & \text{otherwise} \end{cases}$$

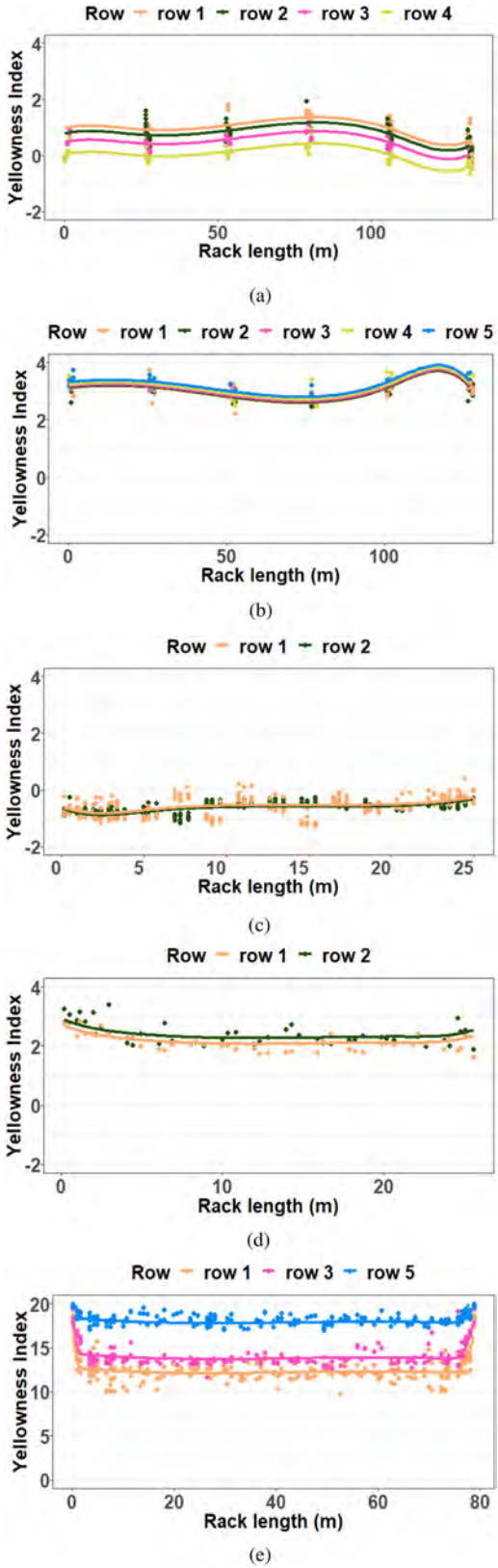

Fig. 2. YI and the generalized spatio-temporal model superimposed on the data, for sites I (a), II (b), III-brand M (c), III-brand N (d), and IV (e). Points represent the measured data and the solid line represents the model. Note the scale of y axis in plot (e) is different than the other plots. (a) Site I (b) Site II (c) Site III-brand M (d) Site III-brand N (e) Site IV.

TABLE II
COEFFICIENTS, KNOTS, ADJUSTED-R^2, AND RMSE OF THE GENERALIZED SPATIO-TEMPORAL MODEL FOR EACH SITE

Site	**I**	**II**	**III**		**IV**
Brand	K	L	M	N	O
β_0	1.04	3.09	0.24	2.38	17.0
β_1	0.35	0.59	-0.36	-0.37	-4.34
β_2	-0.68	-0.15	-0.32	-0.91	-5.45
β_3	1.21	0.53	-0.38	-0.59	-4.31
β_4	-0.52	-0.10	-0.30	-0.71	-4.92
β_5	-0.43	-0.05	-0.32	-0.40	-0.55
β_6	-0.06	-0.02	-0.42	0.06	-0.03
β_7	-0.07	0.02	0.09	0.02	0.01
β_8	NA	NA	-0.16	0.09	NA
a_1	26.6	39.2	5.00	4.64	2.12
a_2	106	118	19.7	21.3	73.6
adjusted-R^2	0.68	0.59	0.34	0.31	0.89
RMSE	0.29	0.18	0.22	0.33	0.92

and G_i is the ground cover type

$$G_1 = \begin{cases} 1 & \text{if ground cover is grass} \\ 0 & \text{otherwise} \end{cases}$$

$$G_2 = \begin{cases} 1 & \text{if ground cover is gray rock} \\ 0 & \text{otherwise.} \end{cases}$$

L is length (m), D is depth (m), a_1, a_2 are knots, and t is the exposure time (years). The estimated model coefficients, knots, adjusted-R^2, and RMSE for each site are shown in Table II. Note that there is no value estimated for the β_8 for sites I, II, and IV, since there is field survey data for only one point in time.

The adjusted-R^2 values show that the GAM model explains 68%, 59%, and 89% of the variation in the field survey data for sites I, II, and IV, respectively. The relatively low values of adjusted-R^2 of 34% and 31% for different brands of site III is because of the large measurement times on each backsheet and the scattered data in this site. The RMSE values show that the overall error of the model is relatively small compared with the range of YI, which indicates that the model represents a good fit to the field survey data. The model is superimposed on the observed values for all sites in Fig. 2. While the model does fit the original data points it exhibits a curved relationship between backsheet discoloration and rack length in the center.

IV. DISCUSSION

A. Implications of Backsheet Yellowing

Discoloration, such as yellowing, because of PV backsheet degradation can be used as an indicator of a backsheet's sensitivity to local weathering effects, and YI can be used as a sensitive predictor of backsheet degradation in the field. A negative value of YI represents that an object is bluish [33]. For backsheets in site I, II, and III (brand M), the values of YI are relatively constant within the rack level for each site, and no appreciable rack "end effect" is observed for these sites and backsheet materials. For the PV modules of brand N in site III, a higher YI of the backsheets at the rack ends is observed during the two field surveys performed. A large difference between YI of backsheets at the rack ends and at the rack center in site IV is also observed. These differences in YI indicate a faster degradation rate for these backsheet materials under these climatic conditions. Therefore backsheets of these materials may show more severe degradation at the rack ends and fail sooner than the backsheets at the center of the rack.

B. Spatial Variation Along Rack Depth and Rack Length

A convex parabolic shape along the depth of the rack in site II, III, and IV is demonstrated by the positive sign of β_7 for D^2 variable. In particular, the opposite sign of β_6 and β_7 (D and D^2 variables) indicates that there exists a minimum value of backsheet discoloration along the rack depth in site II, III (brand M), and IV, and the position of this minimum ($-\beta_6/2\beta_7$) is near the rack bottom. A concave parabolic shape along the depth of the rack is found for site I, in which the PV modules have backsheets with PVDF as the backsheet air-side material. The quadratic relationship between YI and depth illustrates that the effect of depth is enhanced with longer distances from rack front to back.

With similar exposure times, a significant "end effect" along the length of the rack is observed for site IV with PEN air-side backsheets, and a smaller "end effect" is observed for site III (brand N) with PET air-side backsheets. The magnitudes of these "end effects" arises from the relative sensitivity of PEN in comparison to PET as will be discussed in the next subsection. When surveying a PV power plant, that has never been previously surveyed, the initial value of the YI of the backsheet is not known. Therefore, when there is uniform yellowing along a row, it is not possible to know if the backsheets have degraded over time. Identifying a spatial variation in backsheet properties along a row, provide direct evidence that these backsheets are degrading, and that this degradation is occurring over time. The spatial variation provides evidence of temporal degradation, and its magnitude change can suggest the severity of the degradation in the PV power plant. This spatially nonuniform backsheet degradation is important for PV site designers and for operations and maintenance.

Comparing between backsheet YI values with rear-side irradiance and temperature distributions published in the literature, the similarity between the spatial distributions of yellowing and of rear-side irradiance indicates the role of irradiance in these sites, and total photodose, on backsheet degradation [20], [34]. Previous research shows that small temperature variance of modules in the same rack occurs with modules in the center having higher temperatures [34]. Other research on spatial variations in temperature across a PV rack have reported that the temperature differences between modules in different locations of the same rack is small [20], [35]. Therefore, the role of temperature on spatially nonuniform air-side backsheet degradation is small [34], when compared with the role of rear-side irradiance.

The spatial profile of the rear-side irradiance exhibits a shape similar to the YI profile observed for the backsheets in site IV [20], [36]. The rear-side irradiance is highest at the two ends of

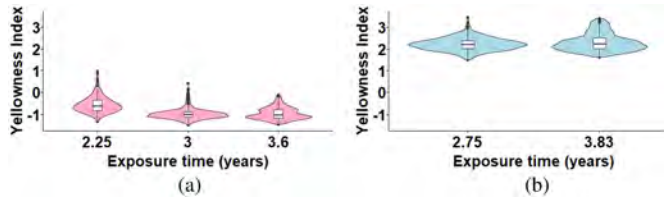

Fig. 3. YI of PET backsheets in site C. (a) Brand "M" (measurement date: December 2016, September 2017, and April 2018). (b) Brand "N" (measurement date: June 2017 and July 2018). The violin plots indicates the distribution of data points.

the rack row and at the top and bottom of the rack, and is also more uniform and increases with higher rack clearance. These are the same characteristics observed in Fig. 2(e). The main factors that affect the intensity of the rear-side irradiance are the reflectivity of the ground cover (referred to as the albedo) and the longitude of the PV site [23]. The UV albedo of ground cover varies $<1\%$ for vegetation to nearly 100% for snow [20], [23], and this strongly affects the degradation rate of the air-side backsheet polymer. In this study, the effect of different ground cover is treated as a categorical variable in the model, and it can be changed to consider the albedo as a numerical variable for use with more balanced field survey data, greater varieties of ground cover, and for the case where the albedo is quantitatively measured at each site. Differences in ground cover materials (e.g., asphalt, concrete, and sand) can lead to changes in temperature and the daily temperature ranges [37]. These ground cover differences represent another degradation stressor and affect the degradation rate of backsheets. Therefore, a PV site should be designed to consider the impact of the rear-side irradiance as much as possible, so as to extend backsheet life.

C. Temporal Dependence of Backsheet Yellowing

The negative coefficient of β_8 indicates the YI of the site III PET backsheets of brand M decreases as the exposure time increases [Fig. 3(a)]. In comparison, the positive value of β_8 for brand N PET backsheets indicates a small increase of YI with increase in exposure time [Fig. 3(b)]. The opposite coefficients of β_8 for these two brands of of PV modules and their backsheets may indicate the different sensitivity of backsheet air-side materials to the same exposure conditions, even for the same type of materials (PET). This could also be attributed to the large differences that arise in formulation of a polymer film for use in a backsheet; for example different grades of TiO_2 (e.g., rutile or anatase phases of TiO_2) or pigment volume concentrations incorporated into PET can lead to distinct degradation mechanisms and yellowing responses. Note that there is no value determined for the β_8 coefficient of sites I, II, and IV since, to date, these sites have been surveyed at one time point.

D. Implication of Backsheet Material Selection

The presence of the rack row "end effect" corresponds to degradation of the backsheet air-side material. In site IV, the air-side backsheet polymer is PEN and has higher YI values (mean $= 15.1$) than those of comparable PET air-side backsheets (mean $= -0.967$ for brand M and 2.17 for brand N) of site III, while these two sites have similar climatic conditions and exposure times. PEN has a similar structure with that of PET except that PEN has a naphthalene ring rather than a benzene ring in its backbone [38]. And the naphthalene dicarboxylate formed during photo-oxidation is the cause of yellowing of PEN. Under the same exposure conditions, discoloration of PEN is faster than that of PET because of the presence of the naphthalene ring, as discussed by Scheirs [38], [39]. The difference of YI values for the two different PV module brands that use PET air-side backsheets may indicate a difference in the pigment volume concentration of TiO_2 used in the PET air-side polymer film, since TiO_2 is a common UV stabilizer for PET, or it can also indicate the addition of brighteners [40], [41]. In addition, PVDF (in site I) has high durability as exhibited by its low yellowing and negligible "end effect" over these exposure times. This negligible "end effect" may arise because of the difficulty to form the long conjugated structures that cause yellowing for the case of PVDF and PA (in site II) while for PET and PEN, the aromatic bonding enables greater yellowing. Therefore, discoloration of PEN backsheets in site IV is more prominent than that observed in site III for PET backsheets with similar exposure times. Here, we report field survey results after four or five years, that in some cases show backsheet degradation in this relatively short exposure time. It is necessary to identify from field surveys and real-world exposure conditions, which backsheets are capable to survive the PV modules product warranty, or its even longer service life. The generalized spatio-temporal model for field surveys of backsheet yellowing will be an effective tool to summarize and standardize the backsheet real-world performance report.

E. Application of the Generalized Spatio-Temporal Model

The estimated parameters of the generalized spatio-temporal model determined for a particular PV power plant site with a particular PV module brand illustrate the quantitative relationship between fielded backsheet degradation and the spatial and temporal variables. According to the values of adjusted-R^2, RMSE, and the superimposed plots, the generalized spatio-temporal model is able to capture the important features of backsheet degradation in these fields. Since the generalized spatio-temporal model provides a simple model equation between backsheet yellowing, exposure time, and the spatial location of backsheet within the PV rack, it can enable PV power plant owners to predict a backsheet's degradation in their PV sites in an efficient manner. In particular, the focus on the backsheets at the two ends of the PV module racks can be considered as the most sensitive location to assess backsheet degradation and the safety of the whole PV site. In addition, more variables, such as the clearance height and the rack tilt angle, which relate to the rear-side irradiance, and the interaction term of time and spatial variables can be added into the generalized spatio-temporal model with more data points from more field surveys to enhance and further broaden the applicability of the model.

The quality and quantity of field survey data, including the number of modules measured, and the number of points in time the field is surveyed, both have a strong influence of the accuracy of estimating the knots location along the rack length in the cubic spline function, which will affect the predictive model's accuracy. The current generalized spatio-temporal model will be more robust with increasing volume of field survey data, and by including field surveys at different time points, as well as by including field surveys of power plants with different backsheet air-side polymers and PV site designs. For the field surveys of sites I and II, an inadequate samplarcing protocol was used, by which there were insufficient measurement points along the rack length, thereby reducing the accuracy of determining knot positions and parameter magnitudes, thereby leading to reduced predictive accuracy. The superimposed plots for site I and II exhibit a local maximum of backsheet discoloration that is not at the rack ends [Fig. 2(a) and (b)] because of the insufficiency of the acquired data and the measurement uncertainty.

It is important to use the appropriate sampling protocol for each field survey so that the more accurate model coefficients can be obtained. In practice, the sample size used in a study is determined based on the expense of data collection and the necessary predictive accuracy needed; this is summarized as the sufficient statistical power based on a statistical test [42]. Given a predetermined Type I error (α) and the effect size, the required number of measurements and field survey can be calculated from the generalized spatio-temporal model based on the current field survey data. In a study of four independent types of materials across three climate zones, the significance of the differences in four materials is being evaluated using the analysis of variance. The total of field surveys for Type I error (0.05) and effect size of 0.55 is 45, which means 15 field surveys would be needed for each material in three climate zones. More field survey datasets with higher temporal and spatial resolution, and greater diversity of backsheet polymers and PV site locations and climate zones are needed to increase the utility of this model to predict backsheet degradation for new PV power plants being designed, installed, and operated.

V. Conclusion

In this study, we developed a generalized spatio-temporal model to predict backsheet degradation based on field survey datasets from real-world PV power plant sites. By the use of a cubic spline and a quadratic function for the rack length and depth predictors, respectively, the generalized spatio-temporal model was able to fit the backsheet degradation data well and captures the two main effects observed; a parabolic relationship of yellowing with rack depth, and a large "end effect" at the two ends of the rack length. PV backsheet degradation is a strong function of the backsheet air-side polymer material and the rear-side UV irradiance distribution, which itself depends on the PV rack's ground cover and clearance. The similarity between the generalized spatio-temporal model with rear-side irradiance points out the importance of irradiance on degradation of backsheets. PV power plant developers can adjust the ground cover, backsheet material and installation position in a PV site, to reduce the predicted backsheet degradation rate and improve and extend the backsheet's lifetime performance, which will contribute to lowering the levelized cost of electricity. In addition, PV power plant owners can quickly assess the sensitivity of their power plant to backsheet degradation by simply surveying the rack ends, to see spatial variations in the backsheet polymer yellowing. The generalized spatio-temporal model helps PV power plant owners estimate which backsheets degrade faster than others in the same field and replace a failed backsheet or module in time to avoid the worse loss. This utility of this spatio-temporal backsheet degradation model will improve over time as more PV fields are surveyed, at more points in time, and as different backsheet polymers are included in survey results.

Acknowledgment

This research made use of the following core facilities and research centers at Case Western Reserve University: the Solar Durability and Lifetime Extension (SDLE) Research Center (Ohio Third Frontier, Wright Project Program Award Tech 12-004), and the High Performance Computing Resource in the Core Facility for Advanced Research Computing.

NIST disclaimer: Certain commercial equipment, instruments, or materials are identified in this work in order to adequately detail the experimental procedure. Such identification is not intended to imply recommendation or endorsement by the National Institute of Standards and Technology, nor is it intended to imply that the materials and equipment identified are necessarily the best available for this purpose.

References

[1] N. Kim *et al.*, "Study on the degradation of different types of backsheets used in PV module under accelerated conditions," *Sol. Energy Mater. Sol. Cells*, vol. 120, pp. 543–548, Jan. 2014.

[2] W. Gambogi *et al.*, "A comparison of key PV backsheet and module performance from fielded module exposures and accelerated tests," *IEEE J. Photovolt.*, vol. 4, no. 3, pp. 935–941, May 2014.

[3] A. G. Klinke, A. Gok, S. I. Ifeanyi, and L. S. Bruckman, "A non-destructive method for crack quantification in photovoltaic backsheets under accelerated and real-world exposures," *Polymer Degradation Stability*, vol. 153, pp. 244–254, Jul. 2018.

[4] C.-C. Lin, P. J. Krommenhoek, S. S. Watson, and X. Gu, "Depth profiling of degradation of multilayer photovoltaic backsheets after accelerated laboratory weathering: Cross-sectional Raman imaging," *Sol. Energy Mater. Sol. Cells*, vol. 144, pp. 289–299, Jan. 2016. [Online]. Available: http://www.sciencedirect.com/science/article/pii/S0927024815004547

[5] M. C. Peel, B. L. Finlayson, and T. A. McMahon, "Updated world map of the Koppen–Geiger climate classification," *Hydrol. Earth Syst. Sci.*, vol. 11, no. 5, pp. 1633–1644, Oct. 2007.

[6] M. Kntges *et al.*, "IEA-PVPS Task 13, SubTask 3.4: Assessment of photovoltaic module failures in the field," IEA-PVPS Task 13, Tech. Rep. T13-09-2017, May 2017.

[7] A. Z. Bradley, J. Kopchick, and B. Hamzavy, "Quantifying PV module defects in the service environment," in *Proc. IEEE 42nd Photovolt. Special. Conf.*, 2015, pp. 1–3.

[8] H. Hu, "Typical photovoltaic backsheet failure mode analysis under different climates in China," in *Proc. Singapore Nat. Eye Centre*, Shanghai, China, 2016, pp. 1–20.

[9] A. Fairbrother *et al.*, "Degradation analysis of field-exposed photovoltaic modules with non-fluoropolymer-based backsheets," *Proc. SPIE*, vol. 10370, Aug. 23, 2017, Art. no. 1037003.

[10] P. SnchezFriera, M. Piliougine, J. Pelez, J. Carretero, and M. S. D. Cardona, "Analysis of degradation mechanisms of crystalline silicon PV modules after 12 years of operation in Southern Europe," *Prog. Photovolt.: Res. Appl.*, vol. 19, no. 6, pp. 658–666, Sep. 2011. [Online]. Available: https://doi.org/10.1002/pip.1083

[11] C. Peike *et al.*, "Impact of permeation properties and backsheet-encapsulant interactions on the reliability of pv modules," *ISRN Renewable Energy*, vol. 2012, 2012, Art. no. 459731.

[12] G. J. Jorgensen *et al.*, "Moisture transport, adhesion, and corrosion protection of PV module packaging materials," *Sol. Energy Mater. Sol. Cells*, vol. 90, no. 16, pp. 2739–2775, Oct. 2006. [Online]. Available: https://doi.org/10.1016/j.solmat.2006.04.003

[13] A. Woyte *et al.*, "Analytical monitoring of grid-connected photovoltaic systems—Good practices for monitoring and performance analysis," IEA-PVPS, Tech. Rep. IEA-PVPS T13-03:2014, Mar. 2015. [Online]. Available: http://iea-pvps.org/index.php?id=276

[14] V. Sharma and S. S. Chandel, "Performance and degradation analysis for long term reliability of solar photovoltaic systems: A review," *Renewable Sustain. Energy Rev.*, vol. 27, pp. 753–767, Nov. 2013. [Online]. Available: https://doi.org/10.1016/j.rser.2013.07.046

[15] M. Garca, L. Marroyo, E. Lorenzo, and M. Prez, "Soiling and other optical losses in solar-tracking PV plants in navarra," *Prog. Photovolt.: Res. Appl.*, vol. 19, no. 2, pp. 211–217, Mar. 2011. [Online]. Available: https://doi.org/10.1002/pip.1004

[16] K. Akhmad *et al.*, "Outdoor performance of amorphous silicon and polycrystalline silicon PV modules," *Sol. Energy Mater. Sol. Cells*, vol. 46, no. 3, pp. 209–218, Jun. 1997. [Online]. Available: https://doi.org/10.1016/S0927-0248(97)00003-2

[17] M. A. Quintana *et al.*, "Diagnostic analysis of silicon photovoltaic modules after 20-year field exposure," in *Proc. Conf. Rec. 28th IEEE Photovolt. Special. Conf. (Cat. No.00CH37036)*, 2000, pp. 1420–1423.

[18] T. C. Felder *et al.*, "Optical properties of PV backsheets: Key indicators of module performance and durability," in *Proc. SPIE*, vol. 9179, Oct. 8, 2014, Art. no. 91790P. [Online]. Available: https://doi.org/10.1117/12.2062063

[19] W. Gambogi *et al.*, "Results of fielded module analysis and the development of accelerated module durability test protocols to better predict real-life performance," in *Proc. 29th Eur. Photovolt. Sol. Energy Conf. Exhibition*, 2014, pp. 2471–2476.

[20] A. Fairbrother *et al.*, "Differential degradation patterns of photovoltaic backsheets at the array level," *Sol. Energy*, vol. 163, pp. 62–69, Mar. 2018. [Online]. Available: https://doi.org/10.1016/j.solener.2018.01.072

[21] L. Kreinin *et al.*, "PV module power gain due to bifacial design. Preliminary experimental and simulation data," in *Proc. 35th IEEE Photovolt. Special. Conf.*, 2010, pp. 2 171–2 175.

[22] U. A. Yusufoglu *et al.*, "Analysis of the annual performance of bifacial modules and optimization methods," *IEEE J. Photovolt.*, vol. 5, no. 1, pp. 320–328, Jan. 2015.

[23] R. Chadyiene and A. Girgdys, "Ultraviolet radiation albedo of natural surfaces," *J. Environ. Eng. Landscape Manage.*, vol. 16, no. 2, pp. 83–88, Jun. 2008. [Online]. Available: https://doi.org/10.3846/1648-6897.2008.16.83-88

[24] G. James, D. Witten, T. Hastie, and R. Tibshirani, *An Introduction to Statistical Learning*, vol. 112. New York, NY, USA: Springer-Verlag, 2013.

[25] A. Gok *et al.*, "Predictive models of poly(ethylene-terephthalate) film degradation under multi-factor accelerated weathering exposures," *PLOS ONE*, vol. 12, no. 5, May 2017, Art. no. e0177614. [Online]. Available: https://doi.org/10.1371/journal.pone.0177614

[26] M. P. Murray, L. S. Bruckman, and R. H. French, "Photodegradation in a stress and response framework: Poly(methyl methacrylate) for solar mirrors and lens," *J. Photon. Energy*, vol. 2, no. 1, Nov. 2012, Art. no. 022004. [Online]. Available: https://doi.org/10.1117/1.JPE.2.022004

[27] R. H. French *et al.*, "Degradation science: Mesoscopic evolution and temporal analytics of photovoltaic energy materials," *Current Opinion Solid State Mater. Sci.*, vol. 19, no. 4, pp. 212–226, Aug. 2015. [Online]. Available: https://doi.org/10.1016/j.cossms.2014.12.008

[28] M. Dhimish, V. Holmes, B. Mehrdadi, and M. Dales, "The impact of cracks on photovoltaic power performance," *J. Sci.: Adv. Mater. Devices*, vol. 2, no. 2, pp. 199–209, Jun. 2017. [Online]. Available: http://www.sciencedirect.com/science/article/pii/S2468217917300540

[29] D. A. Gordon, W.-H. Huang, D. M. Burns, R. H. French, and L. S. Bruckman, "Multivariate multiple regression models of poly(ethylene-terephthalate) film degradation under outdoor and multi-stressor accelerated weathering exposures," *PLOS ONE*, vol. 13, no. 12, Dec. 2018, Art. no. e0209016. [Online]. Available: https://journals.plos.org/plosone/article?id=10.1371/journal.pone.0209016

[30] *Standard Practice for Calculating Yellowness and Whiteness Indices from Instrumentally Measured Color Coordinates*, ASTM International Standard E313-15e1, 2015. [Online]. Available: https://doi.org/10.1520/E0313-15E01

[31] S. N. Wood, *Generalized Additive Models: An Introduction with R*, 2nd ed. Boca Raton, FL, USA: CRC Press, 2017.

[32] V. M. Muggeo, "Segmented: An R package to fit regression models with broken-line relationships," *R News*, vol. 8, no. 1, pp. 20–25, 2008. [Online]. Available: http://202.90.158.4/pub/pub/R/doc/Rnews/Rnews_2008-1.pdf#page=20

[33] S. Lampman, *Characterization and Failure Analysis of Plastics*. Materials Park, OH, USA: ASM International, 2003.

[34] T. Elwood and K. Simmons-Potter, "Comparison of modeled and experimental PV array temperature profiles for accurate interpretation of module performance and degradation," in *Proc. SPIE*, vol. 10370, Aug. 23, 2017, Art. no. 1037006. [Online]. Available: https://doi.org/10.1117/12.2274146

[35] M. G. Farr and J. S. Stein, "Spatial variations in temperature across a photovoltaic array," in *Proc. IEEE 40th Photovolt. Special. Conf.*, 2014, pp. 1921–1927.

[36] U. A. Yusufoglu *et al.*, "Simulation of energy production by bifacial modules with revision of ground reflection," *Energy Procedia*, vol. 55, pp. 389–395, Jan. 2014. [Online]. Available: http://www.sciencedirect.com/science/article/pii/S1876610214013368

[37] L. Peck, "Temporal and spatial fluctuations in ground cover surface temperature at a Northern New England site," *Atmos. Res.*, vol. 41, no. 2, pp. 131–160, Jul. 1996. [Online]. Available: http://www.sciencedirect.com/science/article/pii/0169809595000437

[38] J. Scheirs and J.-L. Gardette, "Photo-oxidation and photolysis of poly(ethylene naphthalate)," *Polymer Degradation Stability*, vol. 56, no. 3, pp. 339–350, Jun. 1997. [Online]. Available: https://doi.org/10.1016/S0141-3910(96)00199-1

[39] G. Botelho, A. Queirs, and P. Gijsman, "A comparative study of the mechanism of the thermo-oxidative degradation of poly(ethylene 2,6-naphthalate) and poly(butylene 2,6-naphthalate)," *Polymer Degradation Stability*, vol. 70, no. 2, pp. 299–304, Jan. 2000. [Online]. Available: http://www.sciencedirect.com/science/article/pii/S0141391000001294

[40] K. J. Geretschlger, G. M. Wallner, and J. Fischer, "Structure and basic properties of photovoltaic module backsheet films," *Sol. Energy Mater. Sol. Cells*, vol. 144, pp. 451–456, Jan. 2016. [Online]. Available: http://www.sciencedirect.com/science/article/pii/S0927024815005024

[41] K. D. Weiss, "Paint and coatings: A mature industry in transition," *Prog. Polymer Sci.*, vol. 22, no. 2, pp. 203–245, Jan. 1997. [Online]. Available: http://www.sciencedirect.com/science/article/pii/S0079670096000196

[42] J. Cohen, *Statistical Power Analysis for the Behavioral Sciences*, 2nd ed. Hillsdale, NJ, USA: Routledge, 1988.